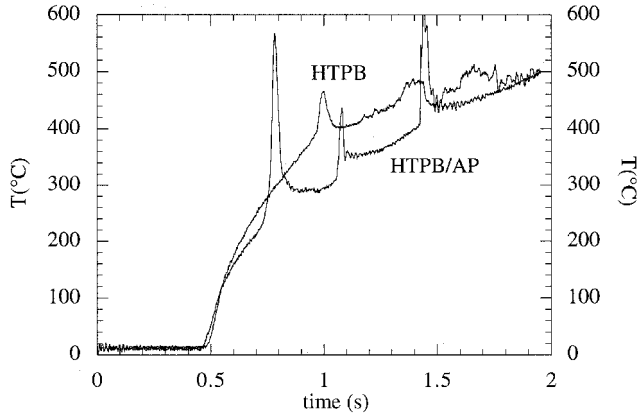

Fig. 1 Effect of fine AP on DDI-cured HTPB decomposition temperature history.

bration measurements showed that the mean laser flux at the position of the sample was 100 W/cm^2. Laser-power output was detected by photoelectromagnetic (PEM) detector monitoring a fraction of the laser beam and recorded.

Results and Discussion

The most significant effect observed in this study was that of including fine AP in the binder. Figure 1 shows the effect of fine AP on decomposition temperature history for DDI curing (similar results were obtained for IPDI). The DDI curve (without AP) shows the typical nonenergetic binder response (similar for IPDI and DDI). For the first 0.5 s of heating, up to 400°C, the temperature follows a profile typical of inert heating, as verified by heat transfer computational simulations. This profile has a steep initial slope that decreases gradually with time. Decomposition begins at 400°C, usually with a rapid, weakly exothermic event, as indicated by a small temperature spike. A significant decrease in the mean slope of the curve also occurs at this point, indicating the onset of a slower, endothermic decomposition process. Further discussion of HTPB decomposition chemistry, including DDI/IPDI, temperature, and pressure effects has been given by Chen and Brill[6] and Arisawa and Brill.[7] In contrast to the pure HTPB behavior, the samples that included AP began decomposing at a lower temperature, between 250 and 300°C, with a rapid, strong exothermic event (first spike in Fig. 1). This was followed by a slower endothermic process as indicated by the slow recovery of the mean profile, whose process was punctuated by additional rapid exothermic events (second and third spikes in Fig. 1). The main significance of these observations is that because AP (lightly pressed powder with no binder) samples did not show the 250–300°C spike, that event must correspond to an exothermic condensed-phase interaction between fine AP and binder. At low heating rates AP exhibits an orthorhomic to cubic phase transition at 240°C associated with free rotation of the perchlorate anions.[8] Perhaps the 250–300°C exothermic event seen in Fig. 1 for HTPB/AP is also associated with the onset of perchlorate ion-free rotation facilitating reaction with the surrounding binder.

Summary

Rapid thermal pyrolysis (10^2–10^3 K/s) was performed on thin film (30–60 μm) mixtures of fine AP and HTPB binder with CO_2 laser energy and simultaneous temperature measurement with foil microthermocouples. A strong condensed-phase chemical interaction was found to occur between fine AP and HTPB as had been previously reported for similar polymers under slow heating conditions.[4] Without AP, endothermic binder decomposition begins at about 400°C, often with a weakly exothermic initiatory event. A significant difference in decomposition was observed with the addition of fine (2 μm) AP: a relatively strong exothermic event occurs at 250–300°C, which is attributed to chemical interaction between fine AP and HTPB (pure AP so rapidly heated does not exhibit this event). This suggests that in the combustion of HTPB propellants containing fine AP, such as wide AP particle size distribution propellants, the condensed phase chemistry between fine AP and HTPB may play a significant role.

Acknowledgments

Funding for this work was provided by the Office of Naval Research (N00014-95-1-1339) and the Ballistic Missile Defense Organization. The authors are indebted to Carol Campbell from Thiokol Corporation for helpful discussions, information, propellants, and other materials.

References

[1]Chakravarthy, S. R., Price, E. W., and Sigman, R. K., "Binder Melt Flow Effects in the Combustion of AP-HC Composite Solid Propellants," AIAA Paper 95-2710, July 1995.

[2]Price, E. W., Shakravarthy, S. R., Sigman, R. K., and Freeman, J. M., "Pressure Dependence of Burning Rate of Ammonium Perchlorate-Hydrocarbon Binder Solid Propellants," AIAA Paper 97-3106, July 1997.

[3]Waesche, R. H. W., and Wenograd, J., "The Effects of Pressure and Additives on the Kinetics of Decomposition of Ammonium Perchlorate," Western States Section, Combustion Inst., WSCI-67-8, East Hartford, CT, April 1967.

[4]Waesche, R. H. W., "Calculation of Solid Propellant Burning Rates from Condensed-Phase Decomposition Kinetics," AIAA Paper 69-145, Jan. 1969.

[5]Isbell, R. A., and Brewster, M. Q., "Optical Properties of Energetic Materials from Infrared Spectroscopy," *Journal of Thermophysics and Heat Transfer*, Vol. 11, No. 1, 1997, pp. 65–71.

[6]Chen, J. K., and Brill, T. B., "Chemistry and Kinetics of Hydroxyl-Terminated Polybutadiene (HTPB) and Diisocyanate-HTPB Polymers During Slow Decomposition and Combustion-Like Conditions," *Combustion and Flame*, Vol. 87, 1991, pp. 217–232.

[7]Arisawa, H., and Brill, T. B., "Flash Pyrolysis of Hydroxyl-Terminated Polybutadiene (HTPB): Implications of the Kinetics and Mechanism to Combustion of Organic Polymers," *Combustion and Flame*, Vol. 106, 1996, pp. 131–154.

[8]Jacobs, P. W. M., and Whitehead, H. M., "Decomposition and Combustion of Ammonium Perchlorate," *Chemical Reviews*, Vol. 89, 1969, pp. 551–590.

Modeling the Effect of Unsteady Chamber Conditions on Atomization Processes

K. M. Rump* and S. D. Heister†
Purdue University, West Lafayette, Indiana 47907

Introduction

THE dynamic behavior of fluid flow through an orifice (injector) brought about by unsteady chamber conditions has been theorized to be a possible explanation for high-frequency combustion instabilities in liquid rocket engines.[1,2] Reba and Brosilow[3] studied the effects of large-amplitude axial acoustic disturbances in the injection chamber on jet breakup length and periodicity of droplet formation for liquids injected into

Presented as Paper 97-3298 at the AIAA/ASME/ASE/ASEE 33rd Joint Propulsion Conference, Seattle, WA, July 6–9, 1997; received July 21, 1997; revision received Jan. 14, 1998; accepted for publication Jan. 23, 1998.

*Research Assistant; currently Staff Engineer, Hughes Space and Communications Company, El Segundo, CA 90254. Member AIAA.

†Associate Professor. Associate Fellow AIAA.

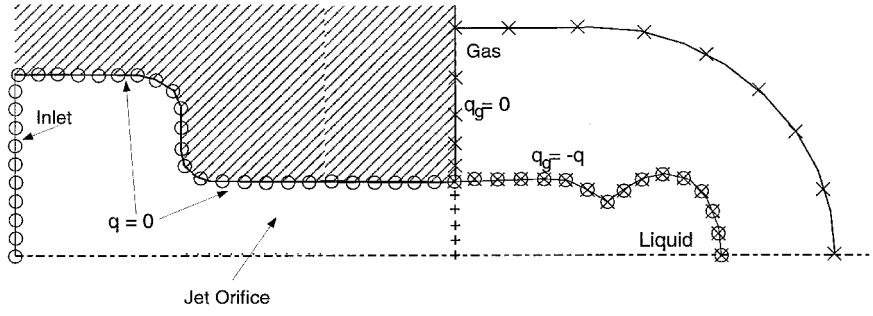

Fig. 1 Schematic of computational domain and boundary conditions.

the chamber. Their observations indicated that the primary factor in determining the distance between drops was the oscillation in the orifice mass flow rate and, therefore, were motivated to develop a simple one-dimensional model for this behavior.

Recently, there have been a number of advancements in the numerical modeling of jet breakup and atomization processes resulting in boundary element method (BEM) models capable of simulating unsteady, nonlinear coupled gas/liquid flows.[4,5] Most relevant to the work described in this Note is a finite length jet BEM developed by Hilbing et al.[4] While that model did not include gas effects, Hilbing did complete preliminary work on a coupled gas/liquid model that was the starting point for the present investigation. This Note will describe the development of the fully coupled model to examine the phase-amplitude response to forced oscillations in the downstream pressure. The effects of orifice length, oscillation frequency and amplitude, and jet injection velocity are addressed through a series of parametric simulations using the model.

Model Development

The model developed for this study uses BEMs to simultaneously solve for conditions in gaseous and liquid phases with the use of a computational mesh containing nodes only on the boundaries of the domain. Both liquid and gas phases are assumed to be inviscid and incompressible, and gravity (or other body forces) are neglected. In addition, the range of acoustic wavelengths studied was assumed to be much larger than the length of the jet such that spatial variations within the chamber gas are negligible and the incompressible assumption is prudent. This assumption is also justified because the injector is typically located near a velocity node and pressure antinode such that minimal spatial variations are present.

The axisymmetric computational domain and boundary conditions used in this model are highlighted in Fig. 1, where q and q_g are velocities normal to the boundary in the liquid and gas domains, respectively. Gas nodes are denoted with $\times$, liquid boundary nodes with $\circ$, and interior nodes with a $+$. The interior nodes permit the calculation of axial velocity within the liquid at the orifice exit plane.[5] Standard inviscid boundary conditions are employed to ensure no flow through solid boundaries and that the pressure jump across the interface is consistent with its current shape.[5] The far-field gas pressure is assumed to vary in time such that the orifice drop ΔP is given by

$$\Delta P = \Delta P_{ss} + \Delta P_{osc} \sin(kt) \tag{1}$$

where ΔP_{ss} is the steady-state pressure drop, ΔP_{osc} is the oscillation amplitude, and k is the oscillation frequency. Studies were conducted to ensure that results were independent of mesh spacing and time steps[5] as a means to validate the code.

Results

A series of 24 simulations were performed to assess the influence of oscillation frequency and amplitude (k, ΔP_{osc}), orifice length-to-radius ratio (l/a), and jet velocity on the orifice mass flow rate response. Jet velocity effects were considered by varying the Weber number ($We = \rho V^2 a/\sigma$), where ρ is the liquid density and σ is surface tension. Computational constraints limited us to consider only low-Weber-number cases; a typical simulation described later in this Note required about 50,000 CPU seconds on an IBM RISC 6000 workstation. Orifice flow rate was calculated by integrating the values of velocity across the inlet boundary and at interior nodes at the orifice exit plane. The flow rate at the two locations was then averaged to provide the results shown in Figs. 2 and 3. Profiles of velocity as functions of radial location within the jet were calculated using the interior velocity calculation procedure de-

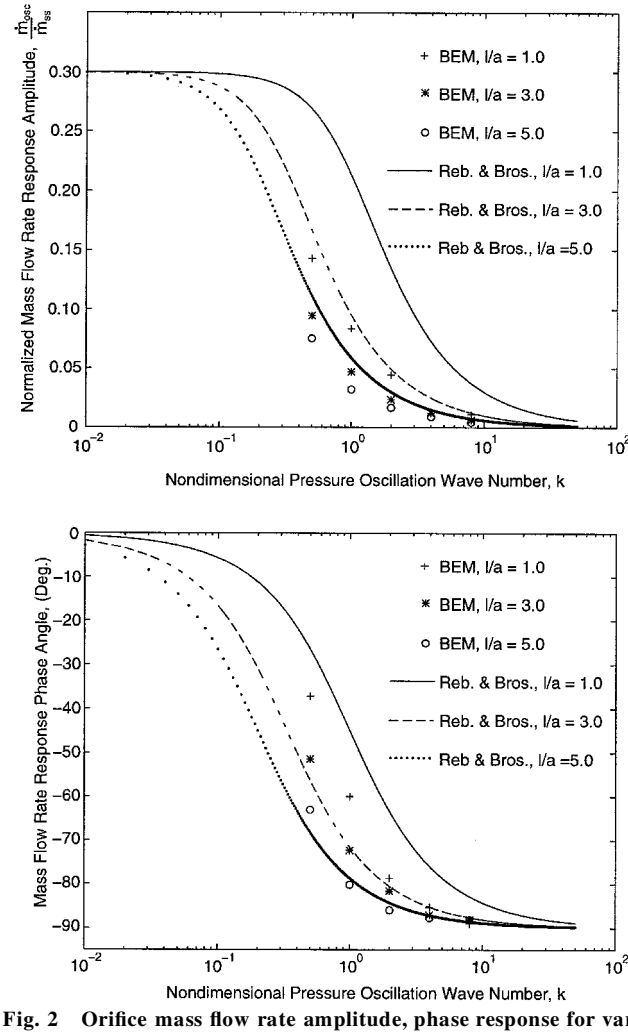

Fig. 2 Orifice mass flow rate amplitude, phase response for various orifice lengths: BEM comparison with analytical predictions for $\Delta P_{osc}/\Delta P_{ss} = 0.5$, $We = 10$.

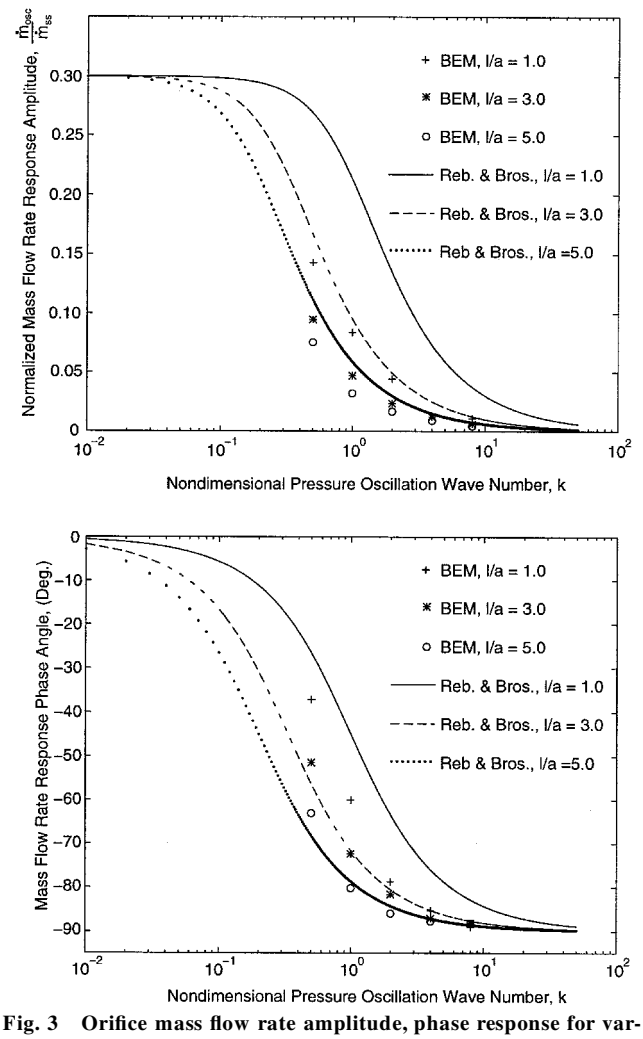

Fig. 3 Orifice mass flow rate amplitude, phase response for various imposed disturbance amplitudes: BEM comparison with analytical predictions for $k = 0.5$, $l/a = 3.0$, $We = 10$.

veloped for this study.[5] A gas/liquid density ratio of 0.01 was used in all of the simulations presented.

In their investigation of liquid jet behavior in the presence of gas-pressure oscillations, Reba and Brosilow[3] derive a one-dimensional, analytical model that can be used to predict the mass flow rate frequency response by performing a momentum balance on the fluid within the orifice passage. The resultant dimensionless orifice mass flow can be written in terms of steady-state $\dot{m}_{ss}$ and oscillatory $\dot{m}_{osc}$ components:

$$\dot{m} = \dot{m}_{ss} + \dot{m}_{osc} = \pi + \frac{\pi \Delta P_{osc} \sin(kt - \alpha)}{\sqrt{(l^2k^2 + 1)}} \qquad (2)$$

ΔP_{osc} is the amplitude of the pressure drop oscillation, and α is the phase lag angle:

$$\alpha = (\pi/2) - \tan^{-1}(1/lk) \qquad (3)$$

Figures 2 and 3 compare flow response predicted using the two-dimensional BEM simulations and the one-dimensional model. A range of frequencies (wave numbers) are considered, $0.1 < k < 10$. Above this frequency range, the jet is unresponsive to the imposed oscillation; below this range a quasisteady behavior is observed. In Fig. 2, the effect of orifice design l/a is considered under fixed excitation amplitude conditions. The two-dimensional BEM results predict more compliance within the injection process than the simple one-dimensional result. As one might expect, the discrepancy is greatest for the short nozzles; at the larger $l/a = 5$ values, the two results are reasonably close. The BEM results also indicate that two-dimensional effects tend to increase the phase lag for the shorter nozzle ($l/a = 1$) as compared to the analytic result. For the longer nozzles, the phase angles for the two approaches agree reasonably well. Both results predict an asymptotic approach to -90 deg as suggested by basic control theory.

Table 1 Comparison of $\dot{m}_{osc}/\dot{m}_{ss}$ and flow rate oscillation phase angle α[a]

We	$\dot{m}_{osc}/\dot{m}_{ss}$	α, deg
5.0	0.211	−63.0
10.0	0.189	−51.4
20.0	0.168	−48.7

[a]For $k = 0.5$, $l/a = 3.0$, $\Delta P_{osc}/\Delta P_{ss} = 0.5$.

Figure 3 addresses the effect of disturbance magnitude ($\Delta P_{osc}/\Delta P_{ss}$) on amplitude and phase lag of the orifice mass flow response for a fixed orifice design ($l/a = 3$). In comparing these results with Fig. 2, we see that the amplitude and phase-angle response is a much weaker function of disturbance amplitude than that of orifice design. In addition, the BEM results suggest a decreased sensitivity to amplitude variation as compared to the analytic predictions. However, both results predict that the phase angle is insensitive to the amplitude of the disturbance.

The effect of Weber number on orifice flow-rate oscillation parameters is displayed for $We = 5.0$, 10.0, and 20.0 in Table 1. Reba and Brosilow's analytical model does not predict any Weber number effects on flow-rate oscillation response amplitude or phase lag because capillary forces are neglected in their derivation.[3] For the low-Weber-number regime investigated in our simulations, results do indicate a strong Weber number dependence on both $\dot{m}_{osc}/\dot{m}_{ss}$ and the phase lag angle α. Physically, the Weber number influence is caused by variations in capillary forces with changes in jet shape. The nonlinear coupling between the jet shape and gas pressure fields leads to the behavior noted in Table 1, i.e., increasing surface tension (decreasing *We*) tends to stiffen the system, but reduces the frequency response.

Because increasing *We* results in smaller response amplitude and phase lag, some of the conclusions regarding phase lag in the discussion of Figs. 2 and 3 may be altered for high-Weber-number conditions. In other words, phase lags for high-velocity jets would be closer to the analytic predictions than those indicated in Figs. 2 and 3. However, Table 1 indicates that phase-angle corrections are asymptotically vanishing in the limit of high Weber numbers, and so the results in Figs. 2 and 3 predict qualitative behavior for the high-Weber-number case.

Conclusions

Two-dimensional BEM simulations have been conducted to assess the dynamic orifice flow under unsteady chamber conditions representative of a liquid rocket engine combustion instability. Results indicate a dynamic orifice response in a range of dimensionless frequencies, $0.1 < k < 10$. Below this lower bound, quasisteady behavior is present, while the orifice is unresponsive above the upper bound.

In general, the two-dimensional effects addressed in the BEM lead to a reduction in the amplitude of the mass flow response as compared to the one-dimensional analytic results. Results are quite sensitive to the orifice length and the increased capacitance effect is most pronounced for shorter nozzles. The two-dimensional results also predict increased phase lags for shorter nozzles; results for long nozzles agree reasonably well with the one-dimensional theory. The two-dimensional results of response of the liquid mass flow show surprising insensitivity to the amplitude of the imposed oscillation in chamber pressure, predicting much less variation than that of the one-dimensional theory. Both one-dimensional theory and two-dimensional simulations show the phase lag to be un-

affected by the magnitude of the imposed one-dimensional oscillation. Variations in Weber number indicate a decrease in both the amplitude and phase lag of the response as *We* is increased.

References

[1]Bazarov, V. G., "Influence of Propellant Injector Stationary and Dynamic Parameters on High Frequency Combustion Stability," AIAA Paper 96-3119, July 1996.

[2]Jensen, R. (ed.), "JANNAF Subcommittee on Combustion Stability—Annual Report," 27th JANNAF Combustion Meeting, Cheyenne, Wyoming, 1990.

[3]Reba, I., and Brosilow, C., "Combustion Instability: Liquid Stream and Droplet Behavior," Wright Air Development Center, TR 59-720, May 1960.

[4]Hilbing, J. H., Heister, S. D., and Spangler, C. A., "A Boundary Element Method for Atomization of a Finite Liquid Jet," *Atomization and Sprays*, Vol. 5, No. 6, 1995, pp. 621–638.

[5]Rump, K., "Modeling the Effect of Unsteady Chamber Conditions on Atomization Processes," M.S. Thesis, Purdue Univ., West Lafayette, IN, 1996.

Near-Critical Liquid Oxygen Droplet Measurements

M. Ferraro,* R. J. Kujala,* J.-L. Thomas,†
M. J. Glogowski,* and M. M. Micci‡
Pennsylvania State University,
University Park, Pennsylvania 16802

Introduction

SUPERCRITICAL droplet evaporation and combustion are some of the least understood processes occurring in current and future aerospace propulsion systems. They occur in current cryogenic rocket motor chambers when oxygen is injected (in the liquid state at supercritical pressure) into a combusting environment that is above its critical temperature while the injected hydrogen gas is already above its critical pressure and temperature. Supercritical droplet evaporation and combustion will also be present in future high-speed airbreathing propulsion systems where the fuel, whether hydrocarbon based or liquid hydrogen, will be used to cool the engine, avionics, and airframe, and will thus be preheated above its critical temperature before injection into the combustion chamber.

Above the critical pressure and temperature, the distinction between liquid and gas phases breaks down as their densities become similar and dramatic changes in material properties occur. For example, the liquid surface tension and heat of vaporization go to zero and the viscosity decreases significantly while the gas solubility into the liquid phase increases. At the same time, knowledge of the droplet lifetimes is essential for the prediction of combustor performance and stability. The droplet lifetime no longer follows the d^2 law and analysis of the process by standard methods, i.e., solution of the Navier–Stokes equations, is difficult because of the highly transient nature of the problem and the need of numerous submodels to obtain the gas and liquid thermodynamic and transport properties.

The Space Shuttle Main Engine (SSME) is one example of a cryogenic hydrogen/oxygen system that operates supercritically. Although the engine has been operating successfully for decades, no knowledge exists of the behavior or characteristics of the liquid oxygen (LOX) subsequent to its injection into the combustion chamber. It is only within the past 15 years that nonintrusive optical means have existed to make spatially resolved measurements of drop sizes and velocities,[1] and even more recently these techniques have been applied to the high-pressure and temperature environments typical of liquid rocket motor combustion chambers.[2] The question has always existed, however, as to what these techniques would measure as chamber pressures and temperatures passed the critical point of the injected fluids.

Experimental Approach

Shear Coaxial Injector Element

The shear coaxial injector for the hot-fire experiments (Fig. 1) permits the modification of critical injector dimensions including the gaseous hydrogen-fuel annulus and LOX post exit areas, LOX post tip landwidth and shape, and the recess depth of the LOX post within the fuel annulus. The baseline dimensions of the injector are derived from the dimensions of the prototype injector element of the fuel preburner to the SSME. These dimensions are summarized in Fig. 1. The fuel annulus segment and LOX post are attached to a main propellant feed segment. A Swagelok compression fitting allows the LOX post to be positioned axially within the fuel annulus. The gas is fed into diametrically opposed inlets on the main-propellant feed segment and accumulated within the relatively large volume of the fuel plenum. To determine the injection properties of the gas, the temperature along with the fluctuating and mean components of the pressure are measured in the plenum region. Likewise, the pressure and temperature of the liquid are measured in the supply line at the entrance to the LOX post. The fuel annulus segment contains a threaded insert that forms the o.d. of the fuel annulus. The insert may be replaced between tests without complete chamber disassembly to change the fuel annulus diameter. The effects of gas-to-liquid velocity ratio, density ratio, and mixture ratio on injector performance may then be studied.

Hot-Fire Experiment

The chamber for these experiments is modular in design, allowing for simple variation of the chamber length, location

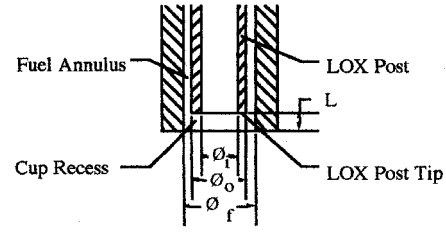

Baseline Dimensions

Fuel Annulus Diameter, $Ø_f$	5.03 mm
LOX Post Outer Diameter, $Ø_o$	3.76 mm
LOX Post Inner Diameter, $Ø_i$	2.26 mm
Post Tip Land Width	0.76 mm
Recess Length, L	2.54 mm

Fig. 1 Shear coaxial injector element schematic with baseline dimensions.

Received March 7, 1997; revision received Jan. 12, 1998; accepted for publication Jan. 20, 1998.

*Graduate Research Assistant, Department of Aerospace Engineering and Propulsion Engineering Research Center. Student Member AIAA.

†Adjunct Research Associate, Department of Aerospace Engineering and Propulsion Engineering Research Center; currently Engineer, Société Européenne de Propulsion, Division Grosse Propulsion Liquide, BP 802,27208, Vernon, France. Member AIAA.

‡Associate Professor, Aerospace Engineering, Department of Aerospace Engineering and Propulsion Engineering Research Center. Associate Fellow AIAA.